J. Fluid Mech. (2010), *vol.* 658, *pp.* 148–165.
doi:10.1017/S0022112010001588

Salt finger fluxes in a laminar shear flow

ALEXANDRE M. FERNANDES[1,2]† AND R. KRISHNAMURTI[1]

[1]Department of Oceanography and Geophysical Fluid Dynamics Institute, Florida State University, Tallahassee, FL 32306, USA

[2]Departamento de Oceanografia Física, Universidade do Estado do Rio de Janeiro, R. São Francisco Xavier, 524, Sala 4017E, Rio de Janeiro, RJ 20550-900, Brazil

(Received 2 September 2009; revised 25 March 2010; accepted 26 March 2010; first published online 28 June 2010)

Subtropical ocean waters are susceptible to the occurrence of salt finger instability. The effect of salt fingers in modifying water mass properties may depend upon the ubiquitous presence of oceanic shear produced by internal wave motion. We present an experimental study of the buoyancy fluxes produced by sugar–salt fingers in the presence of a laminar shear flow. As is commonly done in the laboratory, sugar (the slower diffuser) was used as a proxy for salt, and salt (the faster diffuser compared to sugar) was used as a proxy for cold. Sugar–salt fingers, initially aligned vertically, were observed to tilt when a shear flow was imposed. A consistent decrease in the salt fluxes was measured as the Reynolds number (R_e) was increased by increasing the shear velocity magnitude. Through regression analysis, the salt fluxes were found to depend upon the Reynolds number as $R_e^{-0.025}$, $R_e^{-0.1}$ and $R_e^{-0.34}$, for density ratio values (R_ρ) equal to 1.2, 1.54 and 2.1 respectively. The salt fluxes produced by the sheared fingers were also found to decrease by one order of magnitude when R_ρ increased from 1.2 to 2.1. A computation of the salt Nusselt number revealed that the finger fluxes approach molecular flux values when $R_\rho = 2.1$ and $R_e \simeq 140$.

Key words: double diffusive, low-Reynolds-number flows, mixing enhancement

1. Introduction

The density of seawater is determined by its temperature (T) and salinity (S), as given by the equation of state. The fact that heat and salt diffuse at different molecular rates may lead to the occurrence of a vertical flow across a stably stratified layer of fluid. When the vertical distribution of the faster diffuser (T) is stabilizing and the slower diffuser (S) is destabilizing, such a flow takes place as a result of the salt finger instability (Stern 1960). It takes the form of alternating columns of rising, cold, fresh water and descending, hot, salty water (Schmitt 2003). In this laboratory study, sugar was used as a proxy for salt, and salt was used as a proxy for cold. This avoids the difficulties of dealing with the hard to control heat exchange with the environment. The faster diffuser (salt), however, is still labelled T and the slower diffuser (sugar) is labelled S.

Salt finger activity is important to oceanographers, since it modifies water mass properties. This modified seawater participates in the global thermohaline circulation. Conditions favorable to salt finger occurrence are found in much of the subtropical ocean due to evaporation exceeding precipitation. This produces a warm and salty

† Email address for correspondence: alexmf@gfdi.fsu.edu

water mass at the surface which overlies cooler, fresher water from higher latitudes. In particular, when the ratio of the temperature and salinity contributions to the vertical density gradient ($R_\rho = \rho_0\alpha(\partial T/\partial z)/\rho_0\beta(\partial S/\partial z)$) lies approximately within the interval $1 < R_\rho < 2$, the fingers exist within high gradient density steps O(1–5)m separating mixed layers O(10–100)m in the adjacent fluid. This forms the so-called Thermohaline Staircase, when a series of such layers and interfaces are found with depth (Schmitt 2003). In a staircase, fingers within the high gradient interfaces produce unstable buoyancy fluxes that drive large-scale overturning in the adjacent mixed layers. These fluxes in the ocean, which depend upon vertical temperature, salinity gradients and fluid molecular properties, may also be altered by the presence of internal gravity waves. These waves, which are dominated by near-inertial frequencies, most likely subject the salt fingers to a vertical shear of horizontal velocities.

Observational evidence of salt fingers, possibly affected by an internal wave shear, were reported by Kunze *et al.* (1987) as part of the Caribbean Sheets and Layers Transect project (C-SALT). Shadowgraph images revealed small-scale laminae tilted $\pm 10^\circ$ from the horizontal at finger-favourable density interfaces. Typical height and velocity differences across these interfaces were 2 m and 15–25 mm s^{-1}, respectively, which resulted in a shear $O(10^{-2}\ \mathrm{s}^{-1})$ (Gregg & Sanford 1987). In the North Atlantic Tracer Release Experiment (St Laurent & Schmitt 1999) in the central waters of the North Atlantic subtropical gyre, salt fingers that tilted 10°–20° from the horizontal were often observed at density interfaces with finger-favourable stratification and weak turbulence characterized by density ratio $1 \leqslant R_\rho \leqslant 2$ and Richardson number $R_i \geqslant 1$, respectively.

Tilted salt fingers were also observed in the laboratory by Wells, Griffiths & Turner (2001). In this experiment, a vertically sinusoidal shear was produced while a tank was filled with finger-favourable profiles of sugar and salt solutions. This method produced a sheared flow with a vertical wavelength of ~120 mm and maximum horizontal velocities of about ± 2.5 mm s^{-1}. The vertical velocity of finger growth was computed from the shadowgraph images as 2.5 mm s^{-1}, which resulted in fingers being tilted to 45°.

As described above, the few laboratory and observational studies in the literature indicate that fingers do tilt in the presence of a shear flow. However, much still needs to be known about the fluxes produced by these sheared, tilted fingers. According to our information, the work of Linden (1974) is the first and only systematic laboratory study on the effect of a steady shear flow upon salt fingers. His experiments were carried out on a rectangular channel, in which two layers of fluid were set up in a counterflow arrangement. The tank was divided into an upper and a lower section by a splitter plate. Each section had an inlet at mid-depth that was supplied with fluid at given steady flow rates controlled by constant-head tanks. By withdrawing the splitter plate, the two layers could be set in contact, and the fingers started to form between them, with the shear being produced by the bulk motion of the layers. The salt and sugar fluxes across the interface were estimated by taking conductivity and density measurements of the upper and lower fluid solutions as they left the channel. As for the main goal, the experiments showed that fingers could indeed exist in the presence of a steady shear flow. In terms of finger structure, a linear stability analysis for the small shear of a two-layer finger fluid and finite amplitude calculations revealed that transverse modes, perpendicular to the direction of the mean shear flow, were inhibited, and the preferred mode of instability is a two-dimensional mode parallel to the mean flow (longitudinal modes), named sheets. The existence of these sheets was confirmed in Linden's experiments by top-view shadowgraph images. It was found that the sugar and salt fluxes increased with shear (by increasing the velocity difference

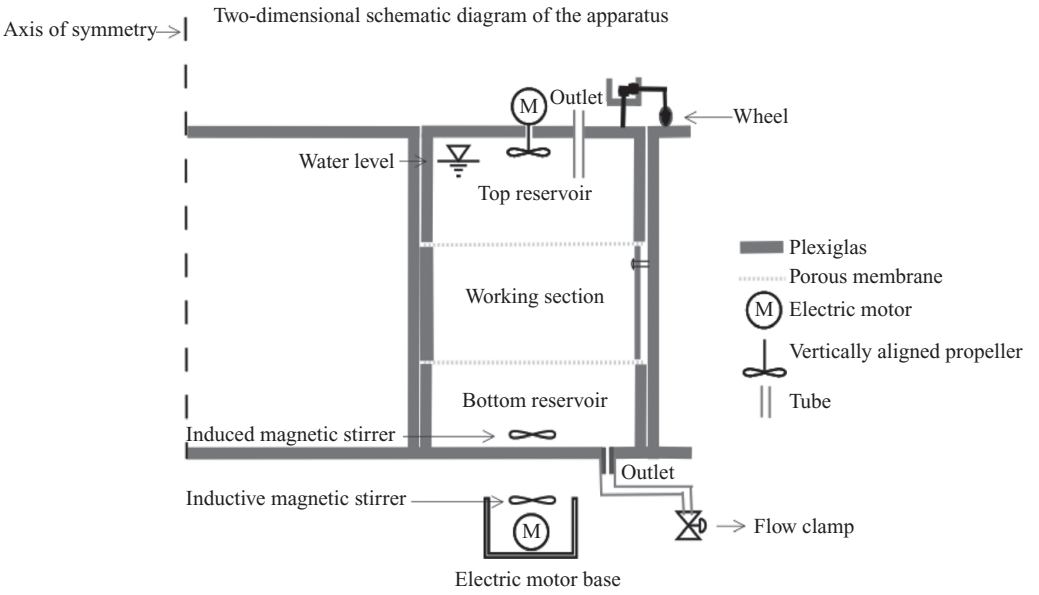

FIGURE 1. Two-dimensional schematic diagram of the apparatus. The top reservoir is set free to rotate counter-clockwise (into the plane of the page) and is supported by small wheels. Below, the finger section and bottom reservoirs stay still.

between the two layers, ΔU). This flux increase, however, was not monotonic for the R_ρ values tested, and sometimes only a slight increasing trend was observed. Attempts to parametrize the finger fluxes were not made.

In the present work, we further explored the effect of a steady shear flow on salt finger fluxes by conducting laboratory experiments to determine a power law which expresses the finger flux dependence on governing parameters. We employed an apparatus with annular geometry that was divided into three sections: a bottom reservoir, an intermediate working section and a top reservoir. In this set-up, the shear was produced by the slow rotation of a rigid boundary (the top reservoir) above the working section that contained fingers. The tank's annular geometry is thought to be a better apparatus design than the one previously employed by Linden for reproducing oceanic sheared finger fluxes in the laboratory, as we will discuss later.

2. Material and methods

2.1. *Apparatus*

A two-dimensional schematic of the experimental apparatus is shown in figure 1. The tank was a 17 cm high Plexiglas annulus with a 44.4 cm diameter at the outer wall and a 20 cm diameter at the inner wall. Inside it were three divided vertical sections: a bottom reservoir, a working section and a top section. Each section was 5.08 cm deep with a radial gap width of 9.5 cm. The sections were separated by 0.010 cm thick porous membranes with a 0.8 μm pore size. These membranes were sheets of Versapor 800 filter that allowed salt and sugar to diffuse through them according to the concentration gradients (Krishnamurti 2003).

During the experiments, the membranes were kept well stretched, and functioned as rigid boundaries separating the fluids. Between the bottom reservoir and the working section, the first membrane was supported by two 4.4 cm high and 0.95 cm thick

Plexiglas rings placed next to the outer and inner walls. An O-ring was fitted in a groove in these Plexiglas rings to hold the membrane taut.

A second Plexiglas annulus was used as the top reservoir. Its inner and outer diameters were properly chosen so that it could be inserted in the top section of the larger annular tank, as shown in figure 1. The second porous membrane was held to this reservoir to separate it from the working section below. The connection between the rotating and the stationary frameworks was made through a slip ring. This device was connected to an electromechanical system that provided unrestrained, continuous rotation while transferring power from a stationary power supply. With this system, the top reservoir could be set to rotate at controlled rates, producing an azimuthal motion of the fluid in contact with the membrane. As a result, a shear flow was formed across the working section with velocities reaching zero at the bottom.

The dimensions of the annular tank were chosen to minimize the curvature effects on the imposed shear flow. By means of a scale analysis of the equations of motion in cylindrical coordinates, the critical non-dimensional parameters were found to be the Reynolds number and annular aspect ratio, given respectively by

$$R_e = \frac{V_0 L}{\nu}, \quad \epsilon = \frac{L}{R}, \tag{2.1}$$

where V_0 is the magnitude of the azimuthal top reservoir velocity at $x = R$ (the radius of the outer cylinder), L is the depth of the working section and ν is the molecular kinetic viscosity of water. This analysis indicated that ϵ should be smaller than one and R_e should be set as close as possible to $O(1)$ in the experiments.

2.2. *Procedure*

In preparing the solutions, we used distilled water, cane sugar and kosher salt. Approximately 525 l of distilled water, 25 kg of sugar and 21 kg of salt were consumed in the 35 experiments performed. Kosher salt was used because it is free of calcium silicate often found in table salt: the former makes clear solutions while the latter does not (Krishnamurti 2003).

The tank was filled in the following way. Initially, two buckets containing salt and sugar solutions were placed 125 cm above the level of the tank. The bottom reservoir was then gravitationally filled with salt solution and the membrane stretched over the fluid to make a flat and rigid bottom for the working section. Care was taken to allow no air bubbles to be trapped under the membrane during this procedure. The working section was then filled with a two-layer fluid. A less dense sugar solution was first poured in and then a denser salt solution was inserted beneath it at a slow filling rate (2.0–2.5 cm h^{-1}). Finally, the top reservoir was inserted in the large annular tank and filled with sugar solution.

The volume of the solutions in the top and bottom reservoirs was the same. In each of these reservoirs, three mechanical stirs were used to keep the solutions well mixed at all times. During the experiments, fluid samples of 50 ml volume were withdrawn from the top reservoir using a syringe. Conductivity, density and temperature readings were taken at 15-minute time intervals and then the samples were returned with the smallest loss of volume possible. The membranes prevented momentum from being transferred across them, and thus the withdrawal and re-insertion of fluid in the reservoirs was carried out without disturbing the flow in the working section. In the bottom reservoir, the measurements were taken to ensure mass conservation. An immersion-probe-type conductivity sensor with a precision of three significant figures and a specific gravity balance with a precision of ± 0.0001 g l^{-1} were used

for conductivity and density measurements, respectively. The conversions to salt and sugar concentration were obtained using the polynomial equations of Ruddick & Shirtcliffe (1979).

The fluxes were computed using a straightforward relation. Calling T^{tr} the salt concentration on the top reservoir, for example, its time rate of change is given by

$$\frac{\mathrm{d}T^{tr}}{\mathrm{d}t} = \frac{F_T}{h}, \tag{2.2}$$

where F_T is the salt flux into the top reservoir, via sugar–salt fingers and diffusion, and h is the depth of the top reservoir. A similar relation applies to the sugar fluxes.

2.2.1. *Velocity measurements*

To determine the velocity profile produced in the working section, the particle image velocimetry (PIV) method was employed. The PIV method is a flow velocity measurement technique in which a plane of laser light is used to illuminate a flow seeded with tracer particles. The particles were silver-coated hollow glass spheres whose density approximately matched that of the fluid being studied. The particle positions were recorded at two different instants of time approximately 1/3 of a second apart. In this procedure, a high-resolution digital camera oriented 90° to the plane of the light was used. Differences in the refractive index of the air ($n_{air} \simeq 1$) and sugar–salt solution ($n_{su} \simeq 1.35$ at 10 % concentration) caused undesirable deviations in the light path from the camera to the annular tank. To minimize this distortion, the tank was placed inside a 50 cm long ($\simeq$10 cm deep) acrylic square tank filled with water. The difference in the refractive index of the water ($n_{water} \simeq 1.33$) and sugar–salt solution is only about 2 %. The recorded images were then analysed using the PIV software (Christensen, Soloff & Adrian 2000) to determine the instantaneous horizontal and vertical flow velocities.

2.3. *Experimental parameters*

In these experiments, we set R_ρ equal to 1.2; 1.54; 2.1. The corresponding values of the sugar Rayleigh number ($R_S = (g\beta\Delta S h_{ws}^3)/(k_T \nu)$) were $R_S \simeq 12\times10^{10}$; 9.4×10^{10}; 7×10^{10}. The initial salt Rayleigh number ($R_T = (g\alpha\Delta T h_{ws}^3)/(k_T \nu)$) was set to $R_T \simeq 4.8\times10^{10}$ and was not varied between experiments. In the expressions above, g is the gravitational acceleration, α and β are the fractional changes in density due to changes in the salt and sugar concentration, respectively, ΔT and ΔS are the initial salt and sugar concentration differences, respectively, $k_T = 10^{-5}\,\mathrm{cm^2\,s^{-1}}$ is the molecular salt diffusion coefficient, $h_{ws} \simeq 5.1$ cm is the working section depth and $\nu = 10^{-2}\,\mathrm{cm^2\,s^{-1}}$ is the kinetic viscosity coefficient of water. The R_ρ values above are within the same range used by Linden (1974) and were adopted here for comparison purposes. The Reynolds number was computed from the top reservoir rotation velocity (ω) as $R_e = (\omega \times r_m h_{ws})/\nu$, where r_m was measured at the mid-radius ($r_m = 17$ cm). The ω values were set approximately within the range of 0 to 0.02 rad s^{-1}. This latter value was found by Krishnamurti & Zhu (1996), using a similar annular tank, to be the limit beyond which radial motions become important.

3. Results

Figure 2 displays two snapshot maps of the velocity vector obtained with the PIV method. The maps correspond to a region approximately 3 cm deep by 1.2 cm wide in the plane of the laser used to illuminate the tracer particles. This plane intercepts the working section at mid-radius ($R \simeq 17$ cm). In both maps a coherent flow to the

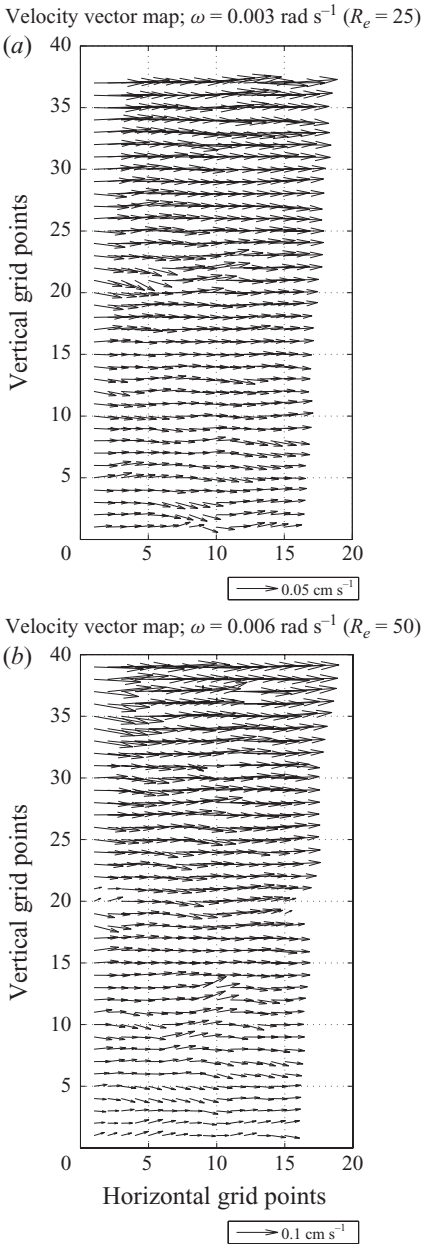

FIGURE 2. Vector maps of the instantaneous velocity in the working section. The maps show a 3 cm depth by 1.2 cm width region; (*a*) $\omega = 0.003$ rad s^{-1} ($R_e \simeq 25$) and (*b*) $\omega = 0.006$ rad s^{-1} ($R_e \simeq 50$).

right, with vector magnitudes decreasing from top to bottom, can be observed. The radial velocity component (not shown) was about two orders of magnitude smaller than the azimuthal component within the range $0 < R_e < 180$.

During many experimental repetitions, qualitative observations were made. By the time we finished filling the reservoirs, the fingers already occupied most of the working section depth. They were 3.5–5 cm tall and approximately 1 mm wide. The rotation

of the top reservoir started right after the filling was finished. The fingers then began to tilt in the direction of the imposed velocity. In the upper millimetres, the fingers were curved. The tilt of the fingers increased as the magnitude of ω increased. This increase also led to a more intense finger curving in their upper regions. The fingers seemed to remain as three-dimensional structures during the experiments.

Figure 3 shows the change with time of the salt concentration measured in the top reservoir for $R_\rho = 1.2$, 1.54 and 2.1. Each curve contained 11–14 data measurements and corresponded to different R_e values. In all plots, a monotonic increase in the salt concentration with time was observed. This is a direct result of vertical salt transport by the fingers. A slight curving of the lines was seen in all plots, which means that the time rate of change of salt concentration changes slightly during the experiments. This curving was more evident when $R_\rho = 1.2$, which corresponded to a more intense vertical transport by the fingers (larger finger fluxes). In this case, the salt concentration (T) in the top reservoir changed from 0 to $\simeq$4.3 p.p.t. in the four-hour duration of the experiments. This corresponded to a reduction of $\simeq$8.4 % of the initial ΔT (51.2 p.p.t.) across the fingers. For $R_\rho = 1.54$, the curving was again observed but with a lower intensity. The initial salt concentration changes from 0 to $\simeq$2.3 p.p.t. corresponded to a change of $\simeq$4.5 %. For $R_\rho = 2.1$, the lines curved slightly upwards. A longer experimental run would more likely show a downward curving similar to that observed for $R_\rho = 1.2$ and $R_\rho = 1.54$. The average change in T, from 0 to 0.8 p.p.t., corresponded to a reduction of $\simeq$1.6 % of the initial ΔT. This smaller change corresponded to a less intense vertical transport by the fingers (smaller finger fluxes) for $R_\rho = 2.1$ than occurred in the previous cases, as was expected for higher density ratios.

A linear fit was performed to determine the slope associated with each salt concentration curve. The time scale, $\tau = h_{ws}^2/\nu$, for the flow adjustment in the working section was estimated to be $\simeq$40 min. Hence, the first three points on each line in figure 3 were not used when computing these slopes. The fluxes were then obtained by multiplying each slope value by the depth of the fluid in the top reservoir ($h = 3.8$ cm). Figure 4 shows the resulting salt fluxes plotted against the Reynolds number. The first point on the left (highest flux value) corresponded to an experiment with no shear imposed ($R_e = 0$). A decrease in the salt fluxes was clearly observed as R_e increased. Deviations from a monotonic decrease were seen in the cases where $R_\rho = 1.2$ and $R_\rho = 1.54$. In the first case, the salt flux fluctuated in the interval $53 < R_e < 122$ while in the latter, a small increase in F_T occurred at $R_e \simeq 75$. These observations might indicate some transitional state in the F_T versus R_e dependence. However, in a few repetitions of these runs, no other evidence of such a transition was observed. For higher R_e values, $R_e \geqslant 200$, which were not explored here, radial motions are expected to become important and may cause a different flux response.

From dimensional analysis, the salt flux F_T may be expressed as

$$F_T = k_T \frac{\Delta T}{h_{ws}} f(R_e, R_\rho, R_T, \tau, P_r), \tag{3.1}$$

where the quantity $k_T(\Delta T)/(h_{ws})$ is the diffusive flux, f is a function of the non-dimensional parameters R_T, R_ρ and R_e, $\tau = k_S/k_T$ is the diffusivity ratio and $P_r = \nu/k_T$ is the Prandtl number. In the sugar–salt system, $\tau \simeq 0.3$ and $P_r = 1000$. A slight decrease of R_T with time during a single experiment occurred owing to the small decrease of the initial ΔT. However, this decrease was less than 10 % and hence R_T was taken as a constant in this analysis. Therefore, for a fixed R_ρ, we express f as a

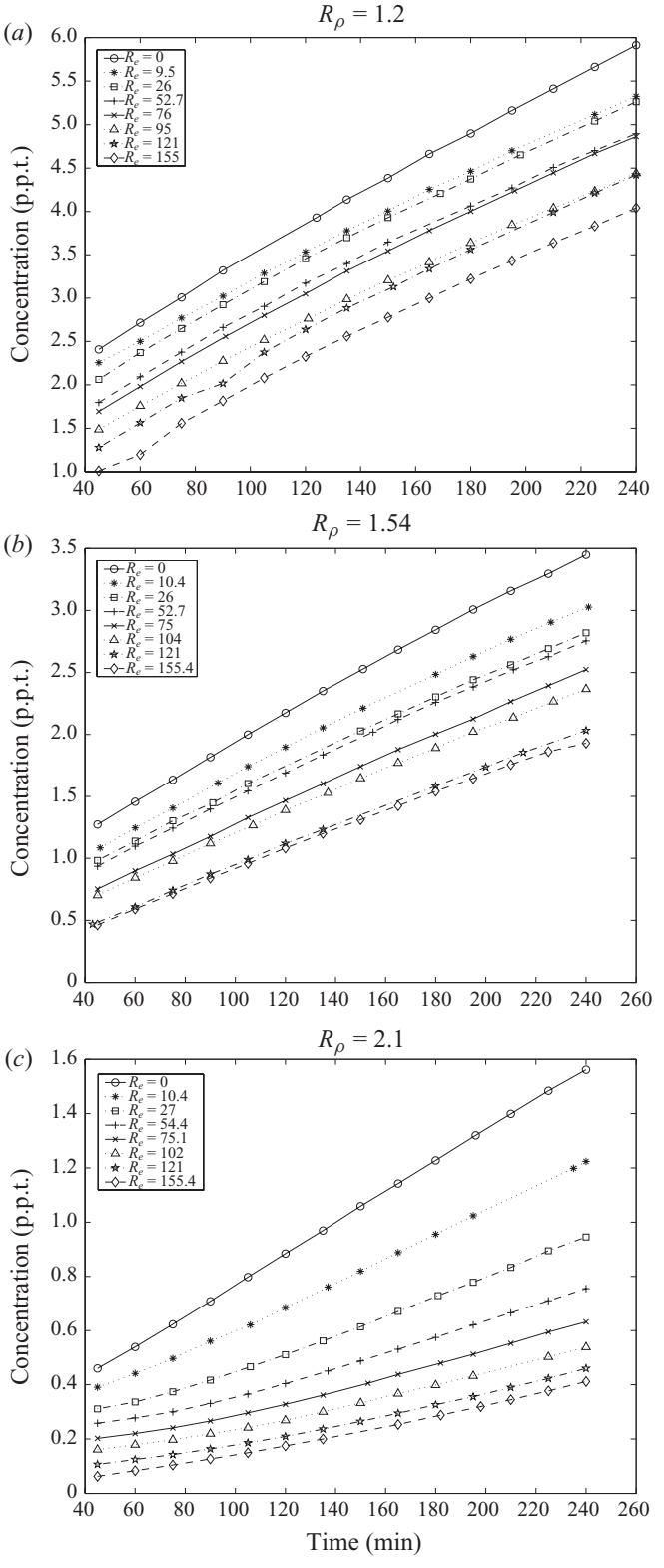

FIGURE 3. Concentration of salt versus time in the top reservoir. The curves are offset by a factor of 0.2, 0.1 and 0.05 p.p.t. for $R_\rho = 1.2$, 1.5 and 2.1 respectively.

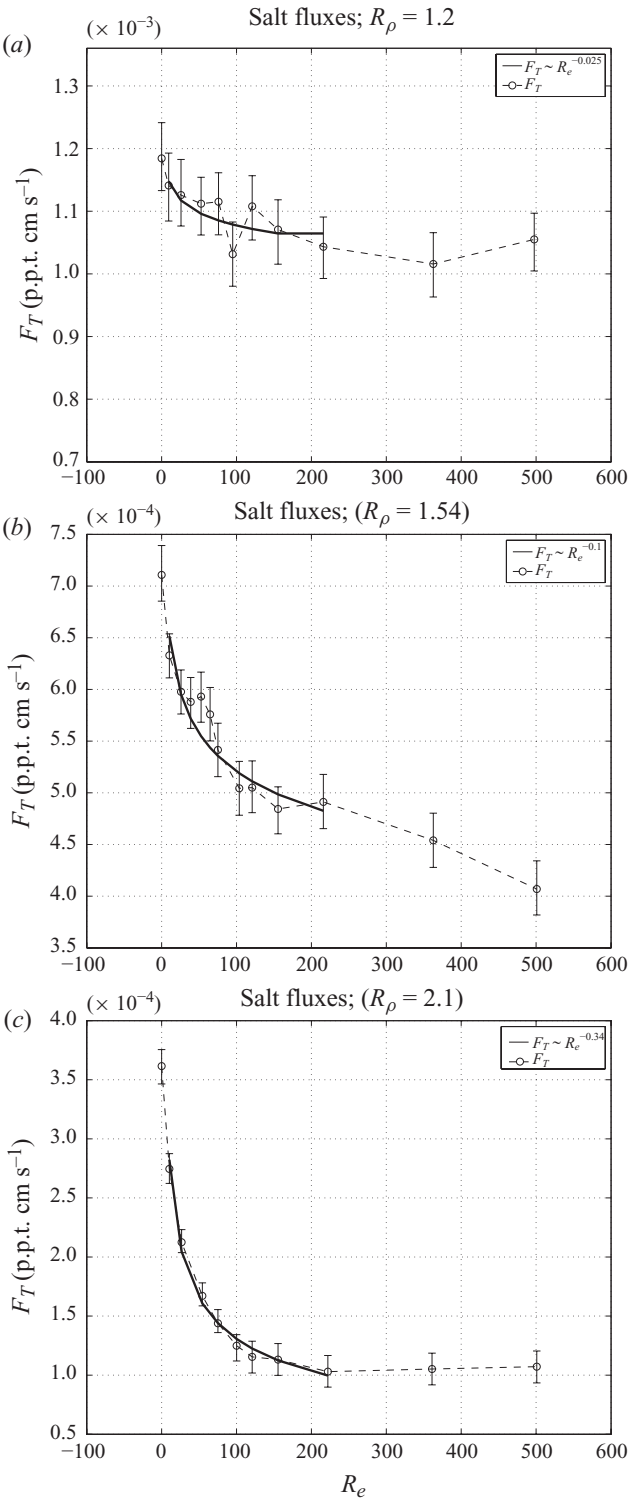

FIGURE 4. Polynomial fit (solid black line) for the salt fluxes.

R_ρ	1.2	1.54	2.1
C	11 ± 0.06	8.1 ± 0.15	6.2 ± 0.2
a	-0.025 ± 0.004	-0.1 ± 0.01	-0.34 ± 0.01

TABLE 1. F_T dependence with R_e for fixed R_ρ values.

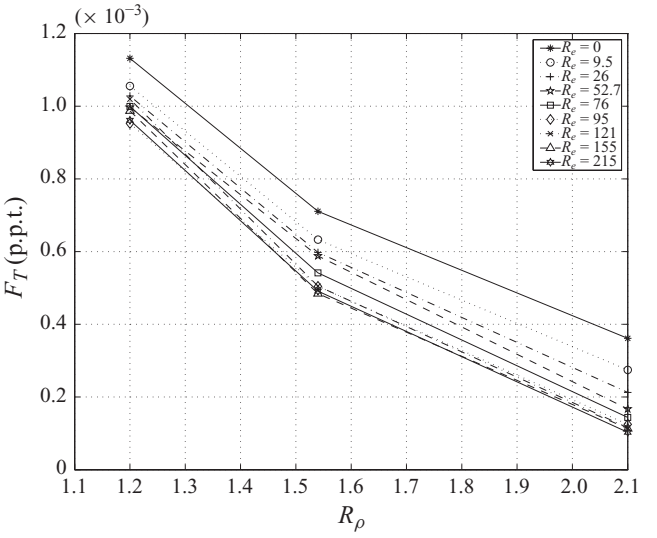

FIGURE 5. The salt flux variation with density ratio for all the experimental runs.

function of R_e only and write this as a power law:

$$f \sim (R_e)^a. \tag{3.2}$$

Hence,

$$F_T \sim k_T \frac{\Delta S}{h_{ws}} (R_e)^a. \tag{3.3}$$

To determine the exponent a, we take the logarithm of equation (3.3) and rearrange it to obtain linear equations:

$$Z_n = a X_n, \tag{3.4}$$

where

$$Z_n = ln(F_T) - ln\left(k_T \frac{\Delta T}{h_{ws}}\right),$$
$$X_n = ln(R_e).$$

A least-squares fit to the data using a linear regression is shown in table 1. These results are displayed in figure 4 and are superimposed on the F_T versus R_e curves. The constants (C) were determined from the graph by eye.

The variations of F_T with R_ρ for fixed R_e values were computed in figure 5. The top curve shows the F_T pattern when $R_e = 0$. In the lower curves, the F_T dependence with R_ρ for sheared fingers follows a pattern similar to the experiments with no shear. In all cases, the F_T values decreased with increasing R_ρ by approximately one order

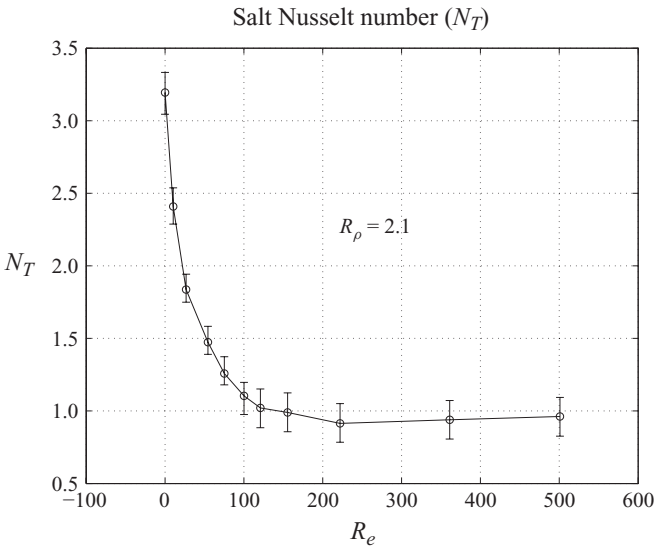

FIGURE 6. Salt Nusselt number versus Reynolds number for $R_\rho = 2.1$.

of magnitude in the range $1.2 < R_\rho < 2.1$. Attempts to include the density ratio on the flux parametrization in (3.3) would have required us to explore a larger number of R_ρ data points. This could have been achieved by employing the method used by Turner (1967) of running through parameter space with the passage of time in his classical run-down experiments. However, with this method, our experiments would last for days and require the use of long-lasting electromechanical devices and a fully automated system for collecting the data, which were unavailable.

Figure 6 shows the salt Nusselt number (N_T), defined as the ratio of the total salt flux measured and the molecular diffusive flux ($N_T = (F_T/k_T)(\Delta T/h_{ws})$) as it varies with R_e for $R_\rho = 2.1$. At this particular value, N_T was seen to range from $\simeq 3.2$ at $R_e = 0$ to 1 at $R_e \simeq 140$, and approached the molecular diffusive flux value, i.e. $N_T = 1$. This low value should be expected at higher R_ρ for experiments with no imposed shear.

As seen in figure 3, the salinity in the top reservoir increased monotonically. Yet, in many repetitions of these experiments, we always found that the density ρ remained unchanged to the fourth decimal place, i.e. the export of sugar out of and the import of salt into the top reservoir compensated for each other. We inferred that the time rate of density change due to sugar concentration ($\rho_o \beta S$) was decreased constantly, as displayed in figure 7. This curious phenomenon was also observed by Krishnamurti (2003) and appears to be related to a chemical bond theory of the density of salt solutions (Dougherty 2001). According to this theory, the addition of salt perturbs the hydrogen bond strength of the water molecules, to cause changes in the density of the salt solutions. However, it is still not clear how this process could compensate for the decrease in the density of the top reservoir solution, which is required to occur by the finger mechanism. This phenomenon should not be expected to hold for all salt concentrations, as verified by Krishnamurti (2003), but that was not the case in our experiments. Owing to this phenomenon, estimates of the sugar fluxes could not be obtained.

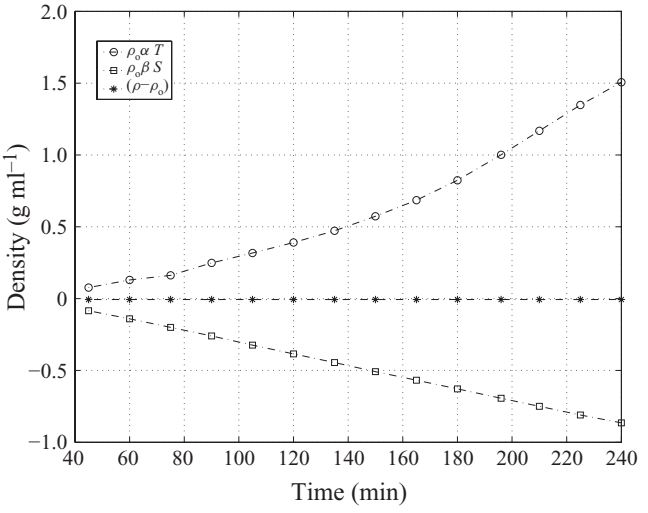

FIGURE 7. Time change of the measured density due to changes in the salt concentration (dashed circles); density (dashed stars); and the inferred density due to changes in the sugar concentration (dashed squares), for $R_\rho = 2.1$ and $R_e = 0$, in the top reservoir solution.

4. Discussion

4.1. *A finger flux reduction mechanism*

The observed decrease in the salt fluxes with increasing R_e may be closely related to the observation that the fingers were seen to tilt in the direction of the imposed shear flow. We discuss this idea, combining a linear stability analysis and the thermohaline staircase model of flux reduction (Krishnamurti 2003).

We used the salt finger model of Howard & Veronis (1987) for the case of no salt diffusion ($\kappa_S = 0$), and computed the density in rising and descending fingers where the equilibrium temperature is given by hyperbolic and trigonometric functions:

$$T = Q\left[\frac{(\cosh x\cos(\pi b - x) + \cos x\cosh(\pi b - x))}{\cosh \pi b + \cos \pi b}\right]. \tag{4.1}$$

In this expression, πb is the finger width and $Q = \beta\Delta S/\alpha L\overline{T}_z$ in rising fingers; the sign is reversed in descending fingers. L is the buoyancy boundary layer thickness:

$$L = \left(\frac{4\nu\kappa_T}{g\alpha\overline{T}_z}\right)^{1/4}, \tag{4.2}$$

where $\overline{T}_z$ is the mean vertical temperature gradient. The salinity in the descending fingers is taken as ΔS and in the rising fingers as $S = 0$.

Calculations show that if negatively buoyant descending fingers are placed horizontally over positively buoyant horizontally placed rising fingers, convective instability will result if the Rayleigh number R (determined by the density difference $\Delta\rho$ between the up- and down-fingers and the finger width, now defined as $\delta/2$) exceeds the critical value R_C:

$$R = g\frac{\Delta\rho\delta^3}{\rho_0\kappa_T\nu} \geqslant R_C. \tag{4.3}$$

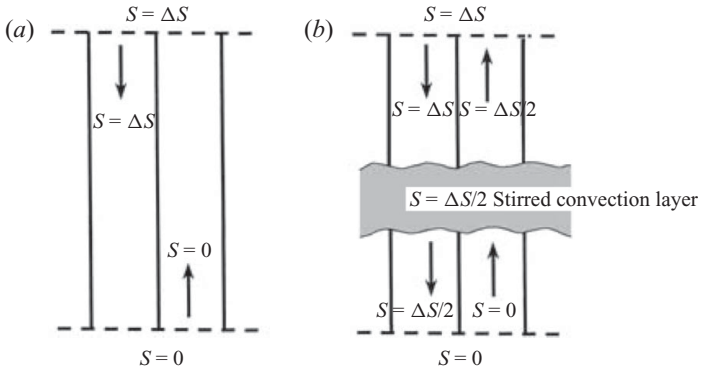

FIGURE 8. From Krishnamurti (2003): schematic representation of the finger flux reduction due to convection. (*a*) Salinity ΔS is exported from the top reservoir via down-fingers, while fresh water ($S = 0$) is imported via up-fingers. (*b*) Salinity ΔS is still exported from the top reservoir, but the import is of salinity $S = \Delta S/2$ resulting from the mixing of up- and down-fingers in the convection layer. Thus half the export is returned, leading to a flux reduction by factor one-half.

If the fingers are not horizontal, but at an angle θ to the vertical, then g may be replaced by $g \sin\theta$ in (4.3). Thus, a critical angle θ_C for convective instability is obtained. Our calculations indicate that $\theta_C \sim 30°$–$40°$ and depends on the density ratio R_ρ and the finger width $\delta/2$.

Linear instability does not imply a flux increase or reduction. However, we argue that stirring by convection, as depicted in figure 8, would result in flux reduction as described by Krishnamurti (2003). The descending fingers carry salinity ΔS from the top reservoir, and the rising fingers carry no salinity from the bottom reservoir (figure 8*a*), resulting in the salt flux F_0. If the up- and down-fingers are perfectly mixed, as in figure 8(*b*), then the rising fingers reaching the top reservoir will have salinity $\Delta S/2$, i.e. half of the ΔS sent down in the descending fingers is returned to the top reservoir, resulting in flux $F_0/2$. In general, if there are n convecting zones, the flux is reduced to F_0/n (Krishnamurti 2003).

Near the onset of instability, $R \geqslant R_C$, the resulting mixing may be less efficient than when $R \gg R_C$. As an indication of this effect, we note that as the angle θ is increased (as observed for higher shear magnitudes in our experiments), the potentially unstable region, where denser fluid overlies less dense fluid, grows in size. The potentially unstable regions are indicated in figure 9 by the hatched shading. In figure 9(*a*) 17 % of the area is potentially unstable, in figure 9(*b*) the value is 30 % and in figure 9(*c*) 70 % is potentially unstable. We therefore suggest this increasing partial instability may account for the monotonic decrease in flux with increasing shear.

We also note that in figure 8 the asymptotic reduction at large shear would be $F_0/2$ if one convection zone fills most of the layer (except where fingers emerge from each boundary). This may be the case at a small enough R_ρ where the destabilizing component is relatively large. On the other hand, the asymptotic reduction in the flux may be $F_0/3$ if the convection is unable to penetrate the two layers (as may be the case for large R_ρ) and the fluid state consists of fingers out of the top boundary, a convection layer below this, fingers at an interface, convection below the interface and fingers at the bottom boundary. The two mixing zones, if thoroughly mixed, would lead to a flux of $F_0/3$. We note from the experiments that the observed fluxes decrease monotonically with the imposed shear (R_e), and the ratio of the observed

R_ρ	$F_n = (F_{R_e 500})/(F_{R_e 0})$
1.2	0.8
1.5	0.6
2.0	0.3

TABLE 2. The salt flux dependence with R_ρ at $R_e = 500$ normalized by the flux at no shear.

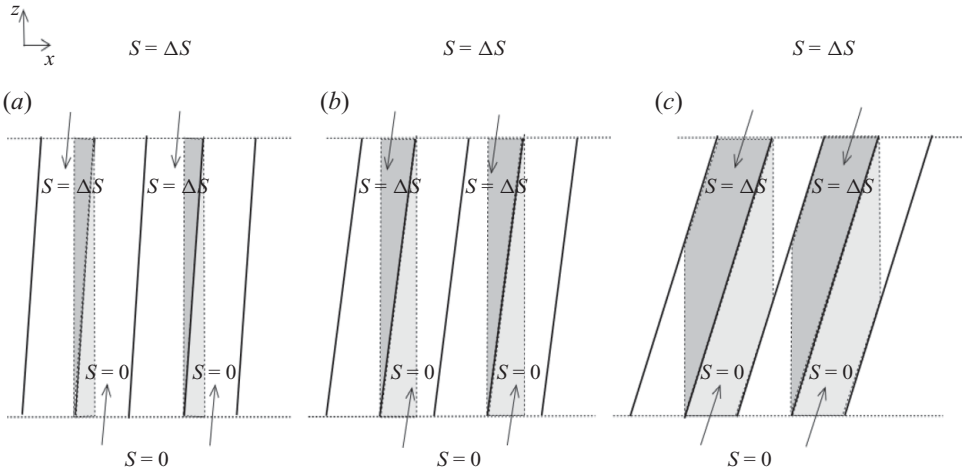

FIGURE 9. Schematic representation of the convecting area (hatched shaded) between two consecutive finger columns. Potentially unstable areas are approximately (*a*) 17 %, (*b*) 30 %, and (*c*) 70 %.

'asymptotic' flux (at $R_e = 500$) to the unsheared flux F_0 varies with R_ρ, as shown in table 2.

Indications of a flux reduction of three-dimensional fingers tilted by an imposed shear flow have been reported by Kunze (1990) for a steady shear, and by Wells *et al.* (2001) for a sinusoidal shear through numerical model calculations. These models, however, have a quite different set-up from the one suggested here, and the flux reduction in their case seems related to a decaying of the effective finger velocity (w) as the angle decreases from the vertical rather than a mechanism of convection between heavier and lighter consecutive tilted fingers. That gives a different dependence of the reduced finger fluxes with the angle. More recently, three-dimensional direct numerical simulations (DNS) of heat–salt fingers interacting with inflectional shear were performed by Kimura & Smyth (2007). Although the primary instability has generated salt sheets aligned with the sheared background flow in their simulations, subsequent mechanisms of secondary instability combined to lead the flow to a turbulent state reducing the effective saline diffusivity.

4.2. *A comparison with Linden's results*

Despite the use of the same range of experimental parameters, different results were found by Linden (1974) and the present study. While the finger fluxes were increased with increasing shear in Linden's experiments, the opposite was observed here. The apparatus geometries may have played a key role in these results. As discussed by Linden, the observed increase in fluxes with increasing ΔU is consistent with the

notion that unsheared salt fingers are in a state of quasi-equilibrium (Linden 1973) with the flux through the fingers being equal to that into the convecting layers on either side. In his experiments with imposed shear, the mean flow advected the sugar and salt brought by the fingers away from the interface region and thereby increase the potential of the convecting layers to take a larger flux from the fingers (Linden 1974). This potential increases with a greater magnitude of shear flow. Thus, the flux increase observed by Linden seems to depend strongly on the way horizontal advection (inlet and outlet of fluid) is imposed to maintain the shear flow in the rectangular apparatus. In his experiments, the advection of the initial T and S fluid volume over a finite horizontal finger region does not resemble the ocean scenario, which is characterized by long horizontal layers with homogeneous T and S properties. This realization also led Linden to conclude that, in the real ocean, finger fluxes should remain unaffected by the presence of a steady shear flow. Despite the shortcoming of having a radial velocity component, which was kept small compared to the azimuthal one in our experiments, the use of the annular apparatus allowed shear to be imposed with no outlet of fluid from the working section, therefore preserving the quasi-equilibrium of fingers and convecting layers. In this sense, the annular apparatus seems a more appropriate choice for studying the fluxes produced by oceanic sheared fingers in the laboratory.

Notable differences between the two studies were also found for the finger structure. The two-dimensional mode (sheets) found by Linden (1974) was not observed in our experiments. Difficulties associated with the deviation of light through an annular tank, plus the fact that the working section was confined between two closed reservoirs, prevented us from conducting a more detailed investigation of the finger structure. From our crude observations with the naked eye, fingers remained three-dimensional in agreement with Wells *et al.* (2001).

We wish to point out that, apart from apparatus geometries, there are other fundamental differences. In our study, the boundary conditions were $u = u_o$ (the velocity of the rigid boundary), $w = 0$ (the vertical velocity), $T = T_o$ and $S = S_o$. The latter two were set by the experimenter at each boundary. In Linden's experiment, the conditions for u, T and S at the interface ($z = 0$) can be expressed as

$$w_1 u_1 + \nu \frac{\mathrm{d}u_1}{\mathrm{d}z} = w_2 u_2 + \nu \frac{\mathrm{d}u_2}{\mathrm{d}z}, \tag{4.4}$$

$$w_1 T_1 + k_T \frac{\mathrm{d}T_1}{\mathrm{d}z} = w_2 T_2 + k_T \frac{\mathrm{d}T_2}{\mathrm{d}z}, \tag{4.5}$$

$$w_1 S_1 + k_S \frac{\mathrm{d}S_1}{\mathrm{d}z} = w_2 S_2 + k_S \frac{\mathrm{d}S_2}{\mathrm{d}z}, \tag{4.6}$$

where indices 1 and 2 refer to values at each side of the finger interface. For initial conditions, we had fingers that were well developed and occupied most of the working section prior to the application of the shear flow, while in Linden's experiments fingers started to grow only after the removal of the splitter plate. As described by Kunze (1990), laboratory experiments reveal that while sheets develop in steady shear they break up into square planform fingers when the shear is turned off. If shear is then re-established, the fingers tilt rather than re-forming sheets. Therefore, fingers are not able to adjust their spacial structure to changing background shear. This would then bring Linden's and the present finger structure observations to an agreement.

Another point that may explain both observations can be related to the non-dimensional parameters. For comparison purposes, we used the same R_ρ and R_e

values as in Linden's experiments. The Richardson number values (R_i) used in both studies were well above critical and their ranges mostly overlap. On the other hand, owing to the observed differences in finger height, $\simeq$3.5–5 cm in our experiments, and $\simeq$0.5–1.5 cm in Linden's, the resulting R_T and R_S overall values were of order 10^{11} in our case and of order 10^9 and lower in Linden's experiments. Although we deal with fingers here, it is worth mentioning that, on Rayleigh–Bénard convection, as the Rayleigh number (R) is increased, the flow structure changes from two-dimensional to three-dimensional (Busse & Whitehead 1971; Krishnamurti & Howard 1981). In this case, further investigations on the sheared finger parameter space would help determine a possible existence of a mode transition.

4.3. *Tilted finger fluxes in the ocean*

As described in § 1, shadowgraph images taken during the C-SALT project revealed fingers tilted by $\pm 10^\circ$ from the horizontal, suggesting the presence of an internal wave shear. Similar tilted fingers were observed during the North Atlantic Tracer Release Experiment (NATRE). As discussed by Kunze *et al.* (1987), by simply kinematic arguments, one might expect the finger orientation to be $\Delta z/\Delta x = w/u$. The 2–3 cm s^{-1} velocity difference across interfaces found in the C-SALT is sufficient to produce tilts up to 86° from the vertical, for typical vertical finger velocities of 0.01 cm s^{-1}. In our experiments, the shear magnitudes imposed across the finger interface were set to be in the same order as those computed in the C-SALT project (10^{-2} s^{-1}). To accomplish that, through a 5 cm finger depth section, the velocity differences imposed across the fingers varied from 0.02 to 0.4 cm s^{-1} approximately. Taking the vertical velocity (w) as equal to 0.01 cm s^{-1}, this would result in fingers tilted by 23° to 63° from the vertical. These values should be even smaller since $w = 0.01$ cm s^{-1} may be overestimated for the less vigorous sugar–salt finger fluxes. In fact, we observed a tilt of about 20°–40° in the present experiments.

The presence of tilted fingers reported in the C-SALT and NATRE projects and associated with low buoyancy fluxes (Greg & Sanford 1987) and absence of staircases (St Laurent & Schmitt 1999), respectively, could be the case of finger fluxes reduced by local internal wave shear. Even in such a case, the overall ability of ocean fingers to produce significant fluxes should not be viewed with scepticism. The more vigorous heat–salt finger fluxes imply higher values of w than for sugar–salt ones. Hence, by the same kinematic reasons described above, one might expect ocean fingers to be less tilted by shear and their fluxes less reduced, according to the mechanism suggested in § 4. Thus, the asymptotic flux reduction at $R_e = 500$, displayed in table 2 for sugar–salt fingers, may be smaller for heat–salt ocean fingers. Also, for the slowly varying near-inertial shear (Kunze 1987), ocean fingers should be expected to quickly re-establish their fluxes. As a matter of fact, the yet unknown relationship between sugar–salt and heat–salt finger fluxes remains a major limitation to possible attempts in developing a parametrization of salt finger fluxes in the ocean.

5. Summary and conclusions

In the present work, we performed laboratory experiments on sugar–salt fingers in the presence of a steady shear flow. A quantitative study was conducted to determine a power law that expresses the salt flux dependence on Reynolds number. The main results are summarized as follows.

(i) The salt fluxes (F_T) decreased with increasing Reynolds number (R_e).

(ii) A flux law describing the F_T dependence with R_e is suggested:

$$F_T(R_\rho = 1.2) = (11 \pm 0.06)\left(k_T \frac{\Delta T}{h_{ws}}\right) R_e^{-0.025\pm0.004}, \tag{5.1}$$

$$F_T(R_\rho = 1.54) = (8.1 \pm 0.15)\left(k_T \frac{\Delta T}{h_{ws}}\right) R_e^{-0.1\pm0.01}, \tag{5.2}$$

$$F_T(R_\rho = 2.1) = (6.2 \pm 0.2)\left(k_T \frac{\Delta T}{h_{ws}}\right) R_e^{-0.34\pm0.01}. \tag{5.3}$$

(iii) The sheared finger fluxes decreased by one order of magnitude when R_ρ increased from 1.2 to 2.1.

(iv) The finger fluxes of salt in the presence of a shear flow approached molecular flux values for $R_\rho = 2.1$ and $R_e \simeq 140$.

Our experiments suggest that, in the ocean, three-dimensional salt fingers should be expected to have their fluxes diminished under steady shear conditions. Even though the present results can not be directly applied to quantify finger fluxes in the ocean, we expect they will help future theoretical and experimental studies and contribute to finger flux parametrizations in general circulation ocean models.

This research was supported by the National Science Foundation under grant number OCE-0242535. The author was funded by the Brazilian Federal Government through the Conselho Nacional de Pesquisa (CNPq). The Geophysical Fluid Dynamics Institute at Florida State University provided the facilities for the development of this work.

REFERENCES

Busse, F. H. & Whitehead, J. A. 1971 Instabilities of convection rolls in a high Prandtl number fluid. *J. Fluid Mech.* **47**, 305–320.

Christensen, K. T., Soloff, S. M. & Adrian, R. J. 2000 PIV sleuth: integrated particle image velocimetry (PIV) interrogation/validation software. *Tech. Rep.* 943. Department of Theoretical and Applied Mechanics, University of Illinois at Urbana–Champaign.

Dougherty, R. C. 2001 Density of salt solutions: effect on ions on the apparent density of water. *J. Phys. Chem.* **105**, 4514–4519.

Gregg, M. C. & Sanford, T. B. 1987 Shear and turbulence in thermohaline staircases. *Deep-Sea Res.* **34**, 1689–1696.

Howard, L. N. & Veronis, G. 1987 The salt-finger zone. *J. Fluid Mech.* **183**, 1–23.

Kimura, S. & Smyth, W. D. 2007 Direct numerical simulation of salt sheets and turbulence in a double-diffusive shear layer. *Geophys. Res. Lett.* **34**, L21610.

Krishnamurti, R. 2003 Double-diffusive transport in laboratory thermohaline staircases. *J. Fluid Mech.* **483**, 287–314.

Krishnamurti, R. & Howard, L. N. 1981 Large-scale flow generation in turbulence convection. *Proc. Natl Acad. Sci.* **78**, 1981–1985.

Krishnamurti, R. & Zhu, Y. 1996 Heat and momentum transport in sheared Rayleigh–Bénard convection. *Physica* D **97**, 126–132.

Kunze, E. 1990 The evolution of salt fingers in inertial wave shear. *J. Mar. Res.* **48**, 471–504.

Kunze, E., Williams III, A. J. & Schmitt, R. W. 1987 Optical microstructure in the thermohaline staircase east of Barbados. *Deep-Sea Res.* **34**, 1697–1704.

Linden, P. F. 1973 On the structure of salt fingers. *Deep-Sea Res.* **20**, 325–340.

Linden, P. F. 1974 Salt fingers in a steady shear flow. *Geophys. Fluid Dyn.* **20**, 325–340.

Ruddick, B. R. & Shirtcliffe, T. G. L. 1979 Data for double diffusers: physical properties of aqueous salt-sugar solutions. *Deep-Sea Res.* **26** A, 775–787.

Schmitt, R. W. 2003 Observational and laboratory insights into salt finger convection. *Prog. Oceanogr.* **56**, 419–433.

Stern, M. E. 1960 The 'salt fountain' and thermohaline convection. *Tellus* **12**, 172–175.

St Laurent, L. & Schmitt, R. W. 1999 The contribution of salt fingers to vertical mixing in the North Atlantic tracer release experiment. *J. Phys. Oceanogr.* **29**, 1404–1424.

Turner, J. S. 1967 Salt fingers across a density interface. *Deep-Sea Res.* **14**, 599–611.

Wells, M. G., Griffiths, R. G. & Turner, J. S. 2001 Generation of density fine structure by salt fingers in a spatially periodic shear. *J. Geophys. Res.* **106**, 7027–7037.